the known carbide clusters can be viewed as derived from an Fe_4C cluster, while the heterometallic nitride cluster can be viewed as derived from an Ru_4N cluster. The metal-metal bonds in the Ru_4 framework are considerably stronger than those in the Fe_4 framework, and substitution of another metal into the Ru_4 framework could have a smaller effect on the overall stability of the metal framework than substitution of a different metal into the Fe_4 framework. Thus, when one Rh atom replaces one Fe atom in $[Fe_4C(CO)_{12}]^{2-}$, the overall perturbation of the electronic structure of the cluster is much larger than when one Fe atom replaces one Ru atom in $[Ru_4N(CO)_{12}]^-$, and it is perhaps not surprising that in the former case one isomer is strongly preferred.

Conclusions

A comparison of the electronic structures of $[Fe_4C(CO)_{12}]^{2-}$, $[Fe_4N(CO)_{12}]^-$, and $Fe_4O(CO)_{12}$ shows that the major consequence of changing the interstitial atom from carbon to nitrogen to oxygen is a significant weakening of the bonds between the interstitial atom and the wingtip metal atoms. Because of the small size of the O atom, the O-Fe interactions may not be sufficient to maintain the same butterfly cluster geometry as that observed for $[Fe_4C(CO)_{12}]^{2-}$ and $[Fe_4N(CO)_{12}]^-$. The $[Ru_4N(CO)_{12}]^-$ anion is found to be isostructural with $[Fe_4N(CO)_{12}]^-$ and $[Os_4N(CO)_{12}]^-$. The only major difference in the electronic structures of $[Fe_4N(CO)_{12}]^-$ and $[Ru_4N(CO)_{12}]^-$ is the increased strength of the metal-metal bonds in $[Ru_4N(CO)_{12}]^-$. The electronic structures of the two isomers of $[FeRu_3N(CO)_{12}]^-$ are found to be very similar. Substitution of Fe into the Ru_4 framework of $[Ru_4N(CO)_{12}]^-$ results in relatively small perturbations of the electronic structure of the cluster, and this probably accounts for the occurrence of the two isomers. Protonation of each of the nitride clusters results in a hydride cluster in which the hydrogen bridges the hinge metal atoms. In each case, this product can be associated with the presence of a high-energy cluster framework bonding orbital that is localized across the hinge of the cluster.

Acknowledgment. The portion of this research that was carried out at the University of Minnesota was supported by a grant from the National Science Foundation.

Supplementary Material Available: Lists of the temperature factors, H atom positions, and all distances and angles (12 pages); a list of the structure factors (22 pages). Ordering information is given on any current masthead page.

Contribution from the Institute for Physical and Theoretical Chemistry, University of Frankfurt, Niederurseler Hang, 6000 Frankfurt am Main, FRG, and Institute for Inorganic Chemistry, University of Witten/Herdecke, 5810 Witten, FRG

Kinetics and Mechanism of the Iron(III)-Catalyzed Autoxidation of Sulfur(IV) Oxides in Aqueous Solution. 1. Formation of Transient Iron(III)-Sulfur(IV) Complexes

Jochen Kraft and Rudi van Eldik*

Received August 3, 1988

The complex formation reactions between aquated Fe(III) and S(IV) oxides were studed spectrophotometrically (UV-vis and FT-IR) and kinetically (stopped flow) under the conditions $5 \times 10^{-4} \le$ [Fe(III)] $\le 6 \times 10^{-3}$ M, $5 \times 10^{-4} \le$ [total S(IV)] $\le 5 \times 10^{-2}$ M, $1.2 \le$ pH ≤ 3.0, $13 \le T \le 40$ °C, and 0.1 M ionic strength. Evidence is reported for the stepwise formation of 1:1, 1:2, and 1:3 sulfito complexes, depending on the pH and [total S(IV)] employed. During the first step $Fe(H_2O)_5OH^{2+}$ is rapidly substituted by HSO_3^-/SO_3^{2-} to produce a 1:1 complex ($K = 600 \pm 30$ M^{-1}), followed by a subsequent substitution at higher [total S(IV)] to produce *cis*- and *trans*-bis(sulfito) species ($K = 40 \pm 20$ and 205 ± 20 M^{-1}, respectively, at 25 °C). These species undergo a second, slower substitution reaction with rate constants of 3.3×10^3 and 4.6×10^2 M^{-1} s^{-1} (pH = 2.5), respectively, to produce a common tris(sulfito) species ($K \ge 650$ and 60 M^{-1}, respectively). The pH dependence of the reactions is accounted for in terms of various acid-base equilibria involving coordinated water and uncoordinated sulfite. The results of this study are discussed in reference to earlier studies reported in the literature.

Introduction

The mechanism of the oxidation of sulfur(IV) oxides by dissolved oxygen in aqueous solution remains unclear, notwithstanding the fact that numerous studies have been devoted to this system.[1,2] This is partly due to the fact that the reported rate laws and rate constants are inconsistent since the reaction is very sensitive to the presence of impurities, especially metal ions that can act as effective catalysts for the oxidation process.[3] In this respect it is important to note that the available kinetic data suggest that the Fe(III)-catalyzed autoxidation of S(IV) oxides can account for up to 80% of the overall oxidation rate at pH = 4-7 in aqueous solution.[2] The general interest in, and efforts to deal with, the acid rain phenomenon in recent years has encouraged us to undertake a detailed kinetic and spectroscopic study of the Fe(III)-catalyzed autoxidation of S(IV) oxides[4] as part of a broader research program dealing with metal-catalyzed atmospheric oxidation processes in general.[5] We now report our results in a series of papers dealing with the formation and decomposition reactions of Fe(III)-S(IV) transients and the overall mechanism in terms of the catalytic activity of aquated Fe(III) in the autoxidation process, respectively.[6] Mechanistic studies of the interaction of transition-metal complexes with the S(IV) oxides SO_2(aq), HSO_3^-, and SO_3^{2-} in aqueous solution have been performed by various groups,[7] especially by Harris and co-workers.[7,8] Following their[8] detailed mechanistic studies of the formation and decomposition reactions of transition-metal carbonato complexes, produced during the reaction of metal aqua species with CO_2(aq)/HCO_3^-/CO_3^{2-} (see ref 9 for a review on their work), investigations of the corresponding SO_x system were undertaken. The interactions of metal complexes with aquated CO_2 and SO_2 exhibit remarkable similarities.

In general, nonlabile octahedral metal hydroxo species can take up CO_2 and SO_2 to produce carbonato and O-bonded sulfito complexes, respectively.[10,11] The process is reversible, and on

* To whom all correspondence should be addressed at the University of Witten/Herdecke.

(1) Chang, S. G.; Littlejohn, D.; Hu, K. Y. *Science* **1987**, *237*, 756 and literature cited in ref 1 of this paper.
(2) Hoffmann, M. R.; Calvert, J. G. *Chemical Transformation Modules for Eulerian Acid Deposition Models*; Government Printing Office: Washington, DC, 1985; Vol. II (Aqueous Phase Chemistry), U.S. EPA-NCAR Interagency Agreement DW 930237.
(3) Huss, A.; Lim, P. K.; Eckert, C. A. *J. Am. Chem. Soc.* **1978**, *100*, 6252.
(4) Kraft, J. Doctoral Dissertation, University of Frankfurt, 1987.
(5) Project C3 of SFB 233 on "Dynamik und Chemie der Hydrometeore".
(6) Part 2: Kraft, J.; van Eldik, R. *Inorg. Chem.*, following paper in this issue.
(7) van Eldik, R. *Adv. Inorg. Bioinorg. Mech.* **1984**, *3*, 275 and references cited therein.
(8) Joshi, V. K.; van Eldik, R.; Harris, G. M. *Inorg. Chem.* **1986**, *25*, 2229 and references cited therein.
(9) Palmer, D. A.; van Eldik, R. *Chem. Rev.* **1983**, *83*, 651.
(10) van Eldik, R.; Harris, G. M. *Inorg. Chem.* **1980**, *19*, 880.

0020-1669/89/1328-2297$01.50/0

acidification rapid release of CO_2 and SO_2 occurs without metal–oxygen bond breakage.[7,9] O-bonded sulfito complexes undergo various subsequent reactions, including substitution, linkage isomerization, and electron transfer.[7,8,10,12,13] In contrast, labile metal complexes tend to directly produce S-bonded sulfito species during the reaction with the SO_x system.[13-15] It follows that the mentioned reactions may all be of significance to atmospheric oxidation processes involving metal–sulfur(IV) complexes.[16] In this paper we report our results for the complex formation reactions of aquated Fe(III) and $SO_2/HSO_3^-/SO_3^{2-}$ in acidic aqueous solution.

Experimental Section

Materials. All chemicals used in this study were of analytical reagent grade and were used without further purification: $Fe(ClO_4)_3$, $NaClO_4$, $HClO_4$, $Na_2S_2O_5$. The hygroscopic $Fe(ClO_4)_3$ (Ventron) was stored under vacuum in a desiccator (CaO). Its water content under these conditions was determined colorimetrically with sulfosalicylic acid to be $Fe(ClO_4)_3 \cdot 9H_2O$, thus resulting in a molecular weight of 516.2. Commercially available Ar gas for the deoxygenation of solvents and the reaction vessel was purified over an O_2-catalyst column in its reduced form (BASF-BTS pellets). The oxygen content of the purified gas was calculated to be $\leq 1 \times 10^{-4}$ vol %. Doubly distilled, deionized water was deoxygenated by boiling it under an Ar atmosphere for at least 15 min, cooling, and storing under Ar.

Preparation of Solutions. The reactant solutions were prepared by using the deoxygenated water as described above. The reactions were usually performed under an Ar atmosphere, but in some cases in the presence of O_2. In the latter case the Fe(III) solution was saturated with O_2 prior to mixing with sulfite solutions, which were prepared under Ar to prevent spontaneous oxidation. Reactions were performed in a 100-cm^3 thermostated Metrohm titration vessel, of which the five inlets were closed with septa and stoppers. The pH of the test solution was adjusted with the aid of $HClO_4$ or NaOH by using a Radiometer pH meter with an Ingold pH electrode. Although the measured pH is usually defined in terms of the activity of the hydrogen ion, we used the concentration of the hydrogen ion by calibrating the pH electrode with analytically prepared solutions. Buffers were not used in the entire study in order to avoid complexation with the highly labile Fe(III) species. The pH electrode was only dipped into the test solution for short periods of time in order to minimize the diffusion of unwanted ions. pH measurements over longer time periods were performed on samples removed from the reaction vessel via the septum. The ionic strength was adjusted with $NaClO_4$.

The degree of O_2 exclusion with the described apparatus was tested on an Fe(II) solution, which in alkaline medium produces a very oxygen sensitive $Fe(OH)_2$ precipitate. Small traces of oxygen convert the white precipitate to green $Fe^{II/III}(OH)_x$ or black Fe_3O_4. Test solutions showed that $Fe(OH)_2$ is stable under the selected conditions for at least 30 min, after which a slow green coloring is observed over a couple of hours. Airtight syringes were used to sample the test solution for analytical purposes.

Instrumentation. Shimadzu and Perkin-Elmer UV–vis spectrophotometers were used to record spectra and to perform slow kinetic measurements. Rapid-scan spectra were recorded with the aid of an OMA II (Princeton Applied Research) detector coupled to a Durrum stopped-flow instrument. This setup enabled the recording of spectra at 50-ms time intervals. However, its sensitivity was not sufficient to record spectra in the lower UV region. For this purpose single-wavelength measurements were performed on a Durrum stopped-flow instrument as a function of wavelength (usually between 350 and 490 nm). Spectra were constructed by combining absorbance–wavelength data at fixed reaction times. This instrument was also used to perform kinetic measurements. The pH of the reaction mixture was measured immediately after mixing by using a small flow-through cell fitted with a Sigma glass electrode coupled to a Metrohm pH meter. The glass electrode was filled with NaCl to prevent the precipitation of $KClO_4$ when KCl was used. Preliminary rate measurements were performed on a Union Giken stopped-flow instrument, which has a 2-mm optical path and a dead time of ≤0.5 ms, compared to the 2-cm path length and dead time of 4 ms for the Durrum instrument. In this way it was possible to obtain kinetic data for the fastest step of the process, although the shorter optical pathlength caused considerable experimental errors.

FT-IR spectra of the reactant and product solutions were recorded after ca. 200-ms reaction time on a Nicolet 5 SX instrument, using a flow-through cell. The latter consisted of two KRS-5 windows (H_2O-insoluble TaBr/I crystals) with an optical pathlength of 0.06 mm, through which the reaction mixture was forced at ca. 30 cm^3 min^{-1}. The recorded spectrum was the mean of between 64 and 128 singly recorded traces.

Rate Measurements. All kinetic measurements were made at an ionic strength of 0.1 M ($NaClO_4$ medium), over the acidity range $1.2 \leq pH \leq 3.0$ and a temperature range of 13–40 °C. No buffers were employed, as mentioned above, and the reactant solutions showed no significant pH drift during the first 30–60 s after mixing. Rate constants were in general measured under pseudo-first-order conditions, and the corresponding first-order plots were linear for at least 2–3 half-lives of the reaction. The reported rate constants were calculated with a standard least-squares program and are mean values of at least five independent measurements.

Data Fitting. In many cases it was possible to find an exact mathematical description to fit the experimental data. In such cases the solid lines and curves in Figures 3–11 represent the calculated data on the basis of the fit. Alternatively, in some cases the data are only used to illustrate a specific trend, and there the lines/curves were calculated by using a polynomial fitting procedure.

Results and Discussion

Equilibria in Solution. Aqueous solutions of $Fe(ClO_4)_3$ contain various aquated Fe(III) species depending on the overall concentration, pH, and ionic strength of the medium. Equilibria 1–3

$$Fe(H_2O)_6^{3+} \rightleftharpoons Fe(H_2O)_5OH^{2+} + H^+ \quad K_1 \qquad (1)$$

$$Fe(H_2O)_5OH^{2+} \rightleftharpoons Fe(H_2O)_4(OH)_2^{+} + H^+ \quad K_2 \qquad (2)$$

$$2Fe(H_2O)_5OH^{2+} \rightleftharpoons (H_2O)_4Fe(\mu\text{-}OH)_2Fe(H_2O)_4^{4+} + 2H_2O \quad K_3 \qquad (3)$$

must be taken into account at pH ≤ 3. At higher pH, colloidal suspensions and precipitates of iron hydroxide and oxides are produced, which prevent the spectrophotometric analysis of the system. We have selected the following equilibrium constants for the Fe(III) system at 25 °C and 0.1 M ionic strength: $K_1 = 6.4 \times 10^{-3}$ M (determined in this study; literature values 4.9×10^{-3} M,[17] 6.3×10^{-3} M[18]) $K_2 = 3.2 \times 10^{-4}$ M[17] (3.3×10^{-4} M[18]); $K_3 = 1.7 \times 10^2$ M^{-1}.[19] Model calculations[4] demonstrated that for [total Fe(III)] $\leq 2 \times 10^{-3}$ M the main species present in solution at pH ≤ 3 are $Fe(H_2O)_6^{3+}$ and $Fe(H_2O)_5OH^{2+}$. To decrease the possible interference of the dimeric species even further, the [total Fe(III)] was usually kept at 5×10^{-4} M, where a maximum of 2% can be present as the dimer. At [total Fe(III)] $> 2 \times 10^{-3}$ M, the concentration of the dimer increases exponentially[20] and the solutions are strongly colored from yellow to red with an increasing absorbance at $\lambda \leq 550$ nm. The $Fe(H_2O)_6^{3+}$ and $Fe(H_2O)_5OH^{2+}$ species exhibit characteristic absorptions at 240 and 295 nm, respectively, such that a gradual shift in equilibrium 1 from pH 1.4 to 3.4 is accompanied by isosbestic points at 222 and 270 nm, without any absorbance at $\lambda > 390$ nm at [Fe(III)] $< 1 \times 10^{-3}$ M.

Sulfur dioxide dissolves readily in water to produce "sulfurous acid", which consists mainly of dissolved and hydrated SO_2. The aqueous chemistry of dissolved SO_2 can be summarized by equilibria 4–7. Selected values for the equilibrium constants at

$$H_2O + SO_2(aq) \rightleftharpoons HSO_3^- + H^+ \quad K_4 \qquad (4)$$
"H_2SO_3"

$$HSO_3^- \rightleftharpoons SO_3^{2-} + H^+ \quad K_5 \qquad (5)$$

$$2HSO_3^- \rightleftharpoons S_2O_5^{2-} + H_2O \quad K_6 \qquad (6)$$

$$HSO_3^- \rightleftharpoons SO_3H^- \quad K_7 \qquad (7)$$

25 °C are $K_4 = 1.26 \times 10^{-2}$ M,[10] $K_5 = 5.01 \times 10^{-7}$ M,[10] $K_6 =$

(11) van Eldik, R.; von Jouanne, J.; Harris, G. M. *Inorg. Chem.* **1982**, *21*, 2818.
(12) Spitzer, U.; van Eldik, R. *Inorg. Chem.* **1982**, *21*, 4008.
(13) Kraft, J.; van Eldik, R. *Inorg. Chem.* **1985**, *24*, 3391.
(14) Mahal, G.; van Eldik R. *Inorg. Chem.* **1987**, *26*, 1837.
(15) Mahal, G.; van Eldik, R. *Inorg. Chem.* **1987**, *26*, 2838.
(16) van Eldik R. In *Chemistry of Multiphase Atmospheric Systems*; Jaeschke, W., Ed.; Springer-Verlag: West Berlin, 1986; p 541.
(17) Martinez, P.; van Eldik, R.; Kelm, H. Ber. *Bunsen-Ges. Phys. Chem.* **1985**, *89*, 81, 447.
(18) Brown, P. L.; Sylva, R. N. *J. Chem. Soc., Dalton Trans.* **1985**, 723.
(19) Milburn, R. M.; Vosburgh, W. C. *J. Am. Chem. Soc.* **1955**, *77*, 1352.
(20) Ardon, M.; Bino, A. *Inorg. Chem.* **1985**, *24*, 1343.

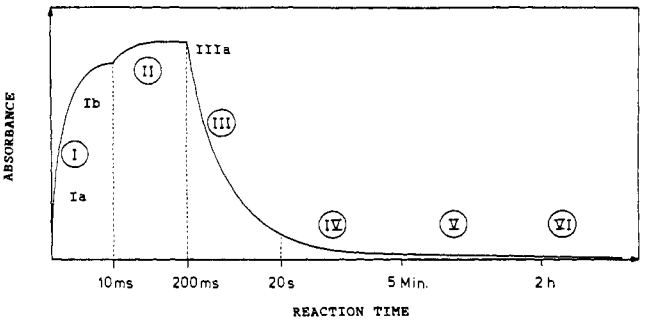

Figure 1. Schematic representation of the absorbance at 390 nm as a function of reaction time during the reaction of aquated Fe(III) with S(IV) oxides. Conditions: [Fe(III)] = 5×10^{-4} M, [total S(IV)] = 1×10^{-2} M, T = 25 °C, pH ≈ 2.5.

8.8×10^{-2} M^{-1},[21] and $K_7 = 4.9$.[22] According to the values of K_4 and K_5, the main S(IV) oxides at pH < 4 will be SO_2(aq) and HSO_3^-. The disulfite species $S_2O_5^{2-}$ is formed at high concentrations of HSO_3^-, but the magnitude of K_6 is such that solutions of $Na_2S_2O_5$ will exist as ≥99% HSO_3^- at $[S_2O_5^{2-}]_T \leq 0.05$ M,[10] a condition usually adopted in our experiments. Recently Horner and Connick[22] presented evidence for two isomers of the bisulfite ion: one with the proton bonded to sulfur (HSO_3^-) and the other with the proton bonded to oxygen (SO_3H^-). The more abundant isomer (SO_3H^-) exchanges oxygen atoms with water approximately 500 times faster than the other isomer.

It follows from the above presentation that when aquated Fe(III) and SO_2(aq)/HSO_3^- are mixed under the conditions adopted in this study, it can lead to the formation of a variety of O- and S-bonded sulfito complexes of unknown coordination number and ligand geometry. A combination of spectroscopic and kinetic analyses enables us to reach some definite conclusions concerning the nature of the sulfito complexes produced during such an interaction.

Spectroscopic Observations. The reaction of Fe^{III}(aq) with HSO_3^-/SO_3^{2-} is characterized by the rapid formation of a yellow to red species with absorbance far in the visible region, which slowly decomposes to a colorless product. The formation and decomposition of this transient can be followed by using stopped-flow and rapid-scan techniques with UV–vis detection. A schematic representation of the change in absorbance at 390 nm during a typical reaction is given in Figure 1. As the following treatment will show, the overall reaction can be subdivided into at least four consecutive steps, of which two account for the formation and two for the decomposition of the Fe(III)–S(IV) transients. The first step (I) of the formation process occurs within 5–10 ms and is too fast to be studied with rapid-scan techniques. However, a spectrum of the product formed during this step can be obtained from initial absorbance measurements for the second step (II) recorded on the stopped-flow instrument as a function of wavelength in the range 350–470 nm. Since the second reaction occurs in a few hundred milliseconds, it should in principle be possible to record repetitive-scan spectra for this step by using a rapid-scan system. Preliminary measurements employing an OMA II rapid-scan system[23] indeed demonstrated the formation of a broad absorption shoulder around 390 nm during this step. However, the overall absorbance change for step II is relatively small (see Figure 1) such that detailed information cannot be obtained from such spectra. It turned out that much more accurate spectral information can be obtained from the stopped-flow traces as a function of wavelength, i.e., a point by point spectral analysis. Some typical results obtained in this way are presented in Figure 2.

The product of step I exhibits a shoulder at 430 nm that shifts to 390 nm during step II of the formation reaction (Figure 2a) under the quoted conditions, with isosbestic points at ca. 350 and 470 nm. These spectra are very typical for the investigated system with a high absorbance, $\epsilon \gg 10^3$ M^{-1} cm^{-1}, in the UV region and a shoulder in the visible part of the spectrum. Parts b and c of Figure 2 demonstrate that the spectral changes are significantly different at higher [total S(IV)], indicating that the formation reaction involves more than one Fe(III)–S(IV) species. The relative concentration of these species is controlled by the [total S(IV)] and pH of the solution. An increase in [total S(IV)] results in the immediate formation of the maximum absorbance during step I, followed by an absorbance decrease during step II. It is important to note that the kinetic data (reported in the following section) confirm that the absorbance decrease observed in Figure 2b,c indeed belongs to step II of the formation process. These spectral changes can qualitatively be interpreted in terms of the formation of three Fe^{III}–SO_3 complexes, viz. 1:1, 1:2, and 1:3, for which the absorbance of 390 nm follows the pattern $\epsilon_{1:1} < \epsilon_{1:1} + \epsilon_{1:2} > \epsilon_{1:3}$. As will be shown later in this paper, this interpretation is also in good agreement with the observed kinetic trends for steps I and II. Although this assignment may seem speculative, it must be kept in mind that we are dealing with the formation of transients on a subsecond time scale and that most analytical techniques employed to identify such species cannot be used under these circumstances.

The complex formation reaction was also studied with FT-IR spectroscopy by a specially constructed flow-through cell as mentioned in the Experimental Section. A comparison of the spectra recorded for the Fe(III)–S(IV) system with those for the individual components[4] revealed a decrease in the "free" sulfite bands at 1213 and 1106 cm^{-1}. This observation is intrepreted as evidence for the formation of Fe(III)–S(IV) complexes, which should exhibit characteristic bands below 300 cm^{-1}, which could not be detected due to the total absorbance by the solvent (H_2O) below 900 cm^{-1}. In addition, a more intense vibration is observed at 1330 cm^{-1} for the complex, which could point to the formation of an S-bonded species since similar spectra were observed for $[Co(NH_3)_5SO_3]Cl$ and $K_3[Rh(NH_3)_3(SO_3)_3]$.

Kinetic Measurements. The above spectroscopic results indicate that complex formation between Fe^{III}(aq) and S(IV) oxides occurs in two steps, which can be separated kinetically by performing the measurements at different wavelengths. The standard wavelength was selected to be 390 nm, and parallel measurements were performed at 470 nm. Preliminary kinetic measurements demonstrated the importance of the overall absorbance change as an indication of the position of the reaction equilibrium. This quantity will be reported and discussed along with the kinetic data to assist the mechanistic interpretation.

It was extremely difficult to obtain kinetic data for step I of the formation process since the rate of this reaction is faster than the mixing time of ordinary stopped-flow instruments. Nevertheless, it was possible to determine the increase in absorbance during this step (equilibrium after ca. 10-ms reaction time), which is the starting absorbance of step II of the process. These absorbance increases show a linear dependence on [total Fe(III)],[4] demonstrating that no substantial interference of dimeric hydroxo–iron(III) species occurs at [total Fe(III)] < 2×10^{-3} M. At constant [total Fe(III)] and pH, the increase in absorbance shows a nonlinear dependence on the [total S(IV)] as indicated in Figure 3. Analysis of these data in terms of the determination of an equilibrium constant for the formation of the Fe(III)–S(IV) complex by a plot of A versus $\Delta A/[S(IV)]$ (see Figure 4) results in clear evidence for the formation of two complex species, depending on the excess of S(IV) employed. The calculated equilibrium constants are $K_{1a} = 600 \pm 30$ M^{-1} and $K_{1b} = 40 \pm 20$ M^{-1}. Under conditions where Fe(III) is in excess, only a 1:1 complex can be produced, and the corresponding absorbance changes (see Figure 5) result in the formation constant $K_{1a} = 600 \pm 50$ M^{-1}. It follows that step I of the process produces 1:1 and 1:2 Fe(III):S(IV) complexes depending on the excess concentration of S(IV).

Provisional rate constants for step I could be obtained by using a stopped-flow instrument with a 2-mm optical path length, which reduces the mixing time to ca. 0.2 ms. The available data are

(21) Connick, R. E.; Tam, T. M.; von Deuster, E. *Inorg. Chem.* **1982**, *21*, 103.
(22) Horner, D. A.; Connick, R. E. *Inorg. Chem.* **1986**, *25*, 2414.
(23) van Eldik, R.; Harris, G. M. *Inorg. Chim. Acta* **1983**, *70*, 147.

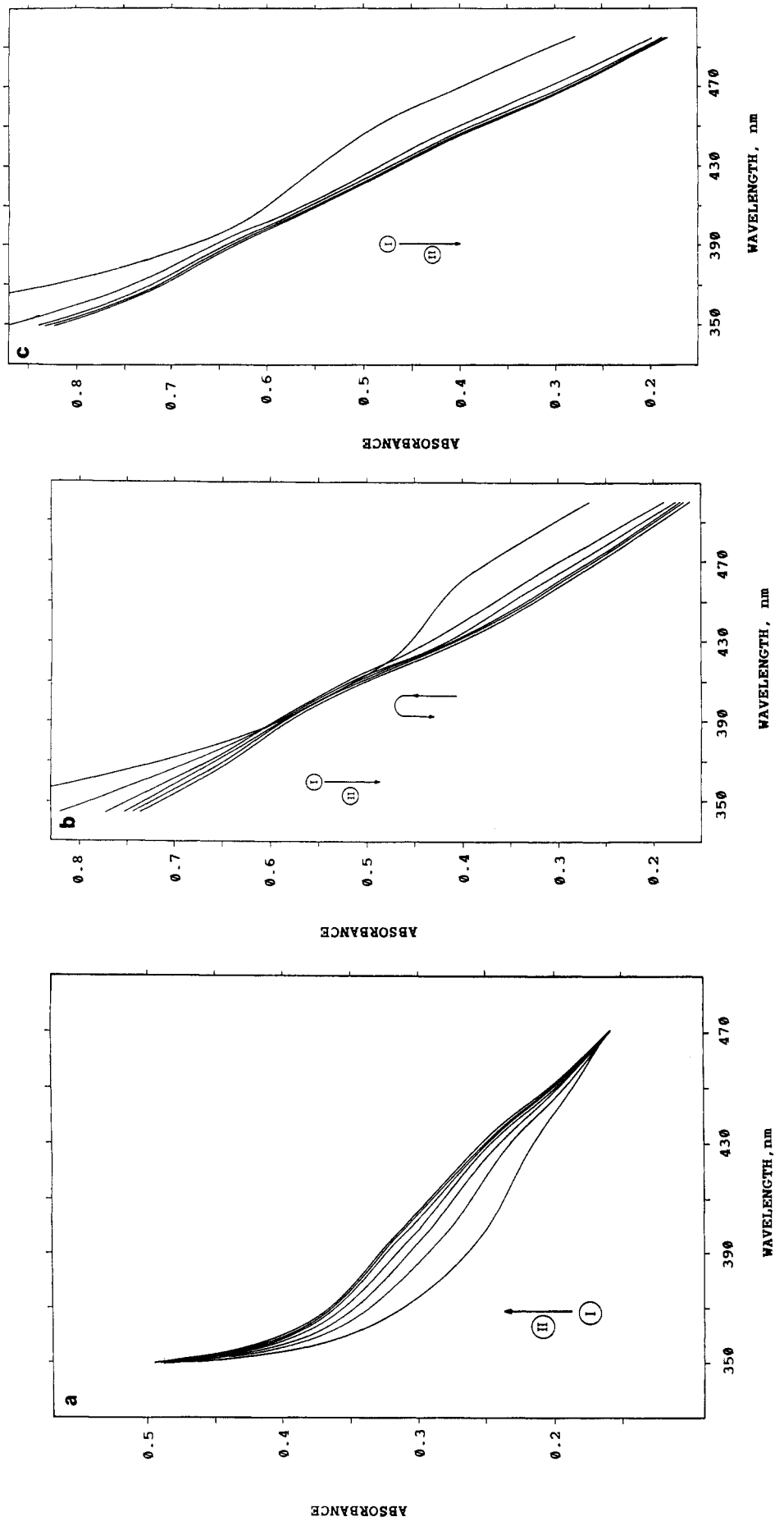

Figure 2. Spectral evidence for the formation of Fe(III)–S(IV) intermediate species during steps I and II. Spectra were constructed from absorbance–time traces. Conditions: $[Fe(III)] = 5 \times 10^{-4}$ M, ionic strength 0.1 M, $T = 25$ °C, pH $\approx$ 2.5, $\Delta t = 50$ ms, optical path length 2 cm, [total S(IV)] = 2.5×10^{-3} (a), 2×10^{-2} (b), 5×10^{-2} M (c).

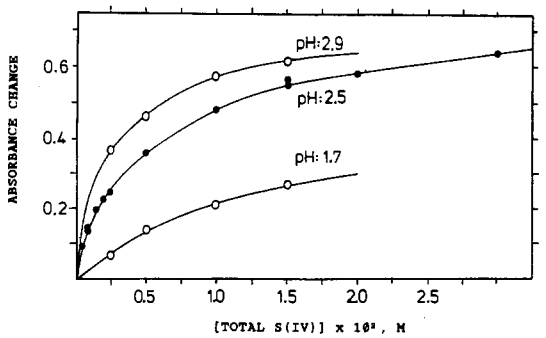

Figure 3. Absorbance change at 390 nm as a function of [total S(IV)] and pH for reaction I. Conditions: [Fe(III)] = 5×10^{-4} M, ionic strength 0.1 M, T = 25 °C, optical path length 2 cm, Ar atmosphere.

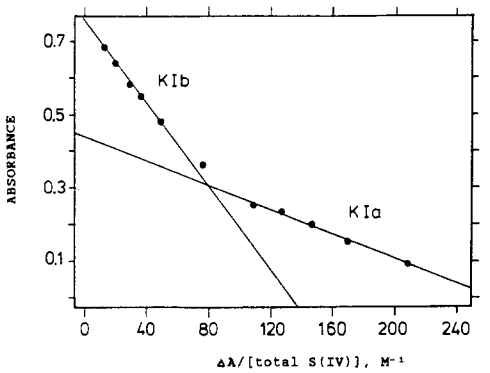

Figure 4. Determination of equilibrium constants for reaction I at pH 2.5 (see text).

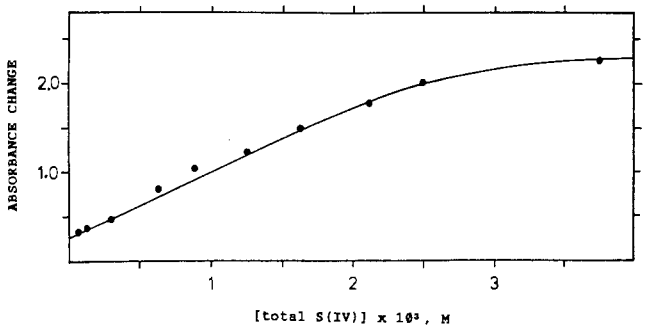

Figure 5. Absorbance change at 390 nm as a function of [total S(IV)] for reaction I. Conditions: [Fe(III)] = 5×10^{-3} M, pH ≈ 2.5, T = 25 °C, ionic strength 0.1 M, optical path length 2 cm, Ar atmosphere.

reported in Figure 6a, from which it follows that k_{obs} (measured at 390 nm) increases significantly with increasing [total (S(IV)]. With the help of the data points at higher [total S(IV)], it is possible to estimate the equilibrium constant $K \approx 12$ M^{-1} at [Fe(III)] = 2×10^{-3} M, which is in fair agreement with the spectrophotometrically determined thermodynamic value of K_{Ib}. However, the large errors involved (due to the relatively small but very fast absorbance change) do not allow a detailed interpretation, although it is likely to assume a strong dependence of k_{obs} on [total S(IV)] at low concentrations. This will lead to a much higher value for K_{Ia} compared to the thermodynamic value of ca. 600 M^{-1}.

The absorbance increase of the rapid reaction Ib, followed at higher [total S(IV)] and 470 nm, exhibits a similar nonlinear dependence (see Figure 6b) as shown in Figure 3. A plot of A versus $\Delta A/[S(IV)]$ results in K_{Ib}(470 nm) = 205 ± 20 M^{-1}, which is significantly larger than K_{Ib}(390 nm) = 40 ± 20 M^{-1}. It becomes obvious that for reaction step Ib two products with different spectral properties and formation constants are produced. Thus, we can conclude that the spectrophotometric and kinetic data suggest the formation of one 1:1 and two 1:2 Fe(III)–S(IV) complexes with formation constants $K_{Ia} \approx 600$ M^{-1}, K_{Ib}(390 nm) ≈ 40 M^{-1}, and K_{Ib}(470 nm) ≈ 205 M^{-1}, respectively. The nature

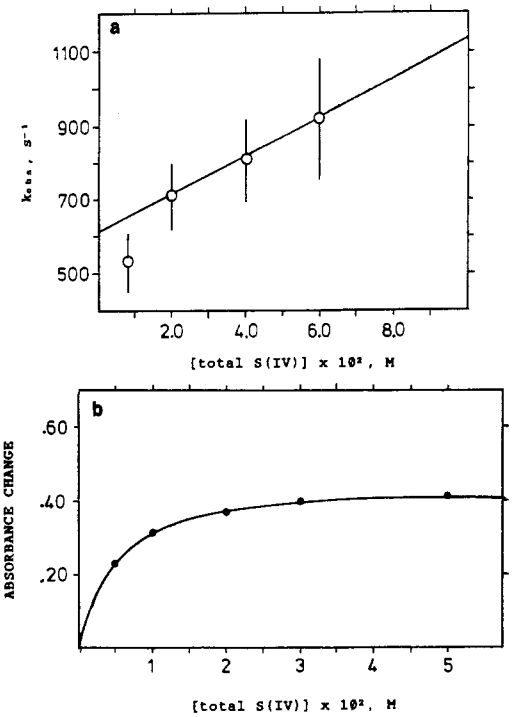

Figure 6. Kinetic and spectroscopic information on step Ib: (a) k_{obs} as a function of [total S(IV)] (conditions: [Fe(III)] = 2×10^{-3} M, pH ≈ 2.5, ionic strength 0.1 M, T = 20 °C, wavelength 390 nm); (b) absorbance change at 470 nm as a function of [total S(IV)] (conditions: [Fe(III)] = 5×10^{-4} M, pH ≈ 2.5, ionic strength 0.1 M, T = 25 °C, Ar atmosphere).

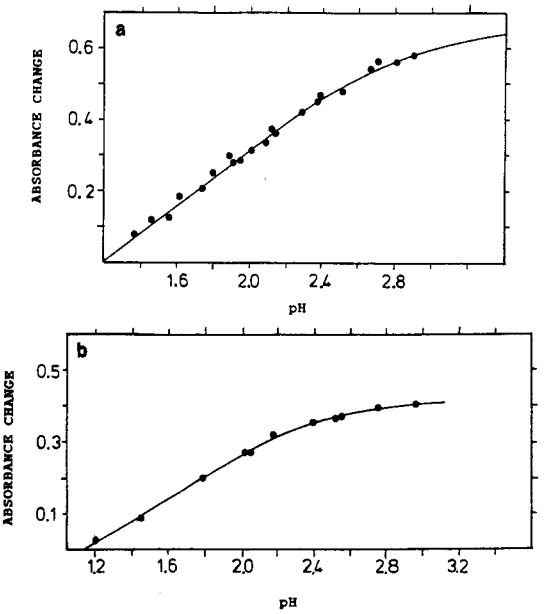

Figure 7. Absorbance change as a function of pH for step I: (a) wavelength 390 nm, [total S(IV)] = 1×10^{-2} M; (b) wavelength 470 nm, [total S(IV)] = 2×10^{-2} M. Conditions: [Fe(III)] = 5×10^{-4} M, ionic strength 0.1 M, T = 25 °C, optical path length 2 cm, Ar atmosphere.

of these species should be revealed by the pH dependence of the observed process. The absorbance increases at 390 and 470 nm are greater with increasing pH as demonstrated by the data in Figure 7. The experiments were limited by the precipitation of hydroxo species at higher pH. Nevertheless, the data show that complex formation during step I reaches a saturation at pH ≈ 3. This can be due to a shift in equilibria 1 and 4 to the $Fe(H_2O)_5OH^{2+}$ and HSO_3^- species, respectively. It is a well-known fact that $Fe(H_2O)_5OH^{2+}$ is ca. 300 times more labile than $Fe(H_2O)_6^{3+}$ at 25 °C,[24,25] such that under the present conditions

(24) Swaddle, T. W.; Merbach, A. E. *Inorg. Chem.* **1981**, *20*, 4212.

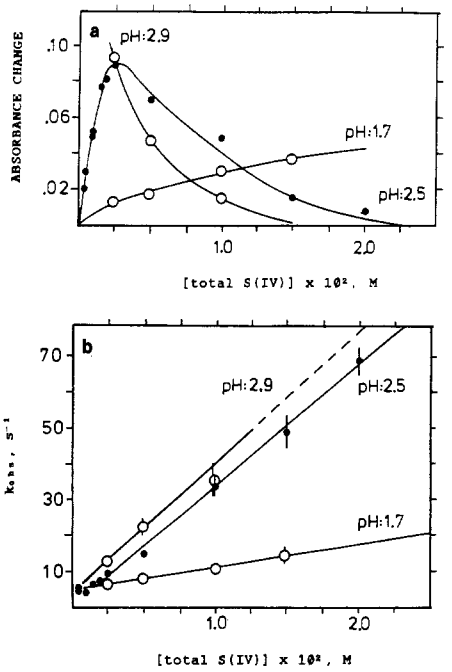

Figure 8. Kinetic and spectroscopic information on step II: (a) absorbance change at 390 nm as a function of [total S(IV)] and pH; (b) k_{obs} as a function of [total S(IV)] and pH. Conditions: [Fe(III)] = 5×10^{-4} M, ionic strength 0.1 M, T = 25 °C, wavelength 390 nm, Ar atmosphere.

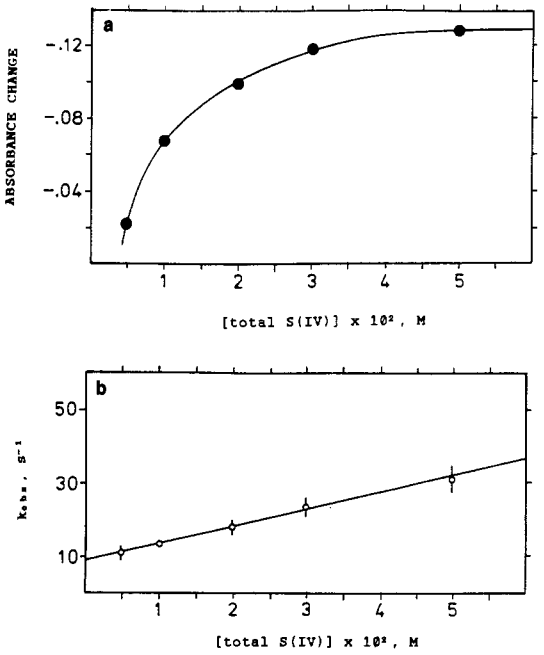

Figure 9. Kinetic and spectroscopic information on step II: (a) absorbance change at 470 nm as a function of [total S(IV)]; (b) k_{obs} as a function of [total S(IV)]. Conditions: [Fe(III)] = 5×10^{-4} M, pH ≈ 2.5, wavelength 470 nm, ionic strength 0.1 M, T = 25 °C, Ar atmosphere.

$Fe(H_2O)_5OH^{2+}$ will be the major reactive species. Furthermore, the lability of this species will favor substitution by HSO_3^- above SO_2 uptake by the hydroxy ligand to produce an S-bonded sulfito complex. The pH dependence of the absorbance increase can therefore be accounted for in terms of the substitution of $Fe(H_2O)_5OH^{2+}$ by HSO_3^-. Experiments were also performed with O_2-saturated solutions, but the measurements (spectroscopic and kinetic) revealed no significant deviations from those reported above, indicating that O_2 does not affect the complex formation step I.

This rapid step is followed by step II, which can be conveniently measured on the stopped-flow instrument. The changes in absorbance at 390 nm for this reaction and the corresponding first-order rate constants are summarized in Figure 8. The maximum in the absorbance–[total S(IV)] plot at pH 2.5 can be understood in terms of the spectral observations discussed in the previous section. Depending on the [total S(IV)] employed, different ratios of the 1:1 and 1:2 complexes are produced during step I such that the formation of the 1:3 complex in step II is accompanied by an increasing or decreasing absorbance change with increasing [total S(IV)], depending on the pH of the solution. An analysis of the spectral changes suggests that $\epsilon_{1:1}$ = 440 M^{-1} cm^{-1}, $\epsilon_{1:2}$ = 760 M^{-1} cm^{-1} and $\epsilon_{1:3}$ = 630 M^{-1} cm^{-1} at 390 nm. The kinetic data for this step show that the slope of k_{obs} vs [total S(IV)] reaches a limiting value at pH = 2.5–2.9, which corresponds to an almost complete shift of equilibria 1 and 4 to the species $Fe(H_2O)_5OH^{2+}$ and HSO_3^-. The small intercept of ca. 5 s^{-1} is presumably due to a back-reaction, indicating that the 1:3 species is in equilibrium with the 1:2 species. From the slope (3720 ± 80 M^{-1} s^{-1}) and the intercept it follows that $K_{II} \geq 650$ M^{-1} at 390 nm. Kinetic and spectroscopic measurements at 470 nm under the same conditions (i.e., [total S(IV)] ≤ 5×10^{-2} M, pH = 2.5) result in K_{II} values of 63 ± 8 (absorbance data) and 53 ± 8 M^{-1} (kinetic data: slope of Figure 9, 460 ± 30 M^{-1} s^{-1}; intercept 8.8 ± 1.0 s^{-1}). This indicates that a different process, most probably involving another complex, as indicated by the two values found for K_{Ib}, is observed at 470 nm. To account for these observations, the suggested mechanism outlined in Scheme I involves the two possible 1:2 complexes (cis and trans) that react at significantly different rates to result in a common 1:3 product (see further discussion).

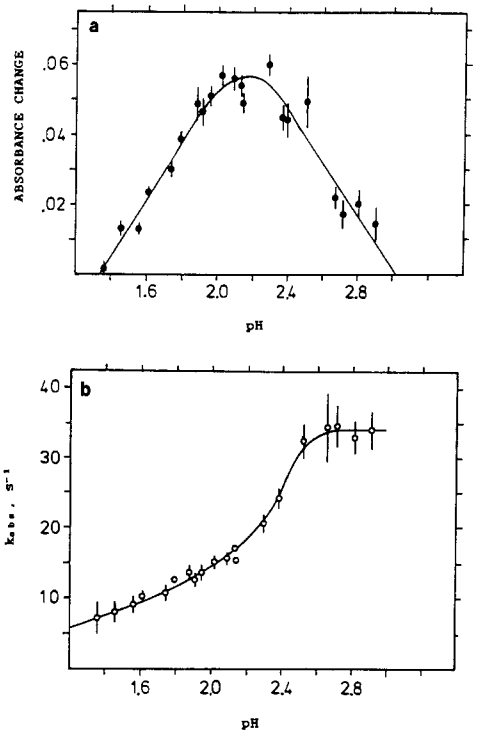

Figure 10. pH dependence of step II at 390 nm: (a) absorbance change as a function of pH; (b) k_{obs} as a function of pH. Conditions: [Fe(III)] = 5×10^{-4} M, [total S(IV)] = 1×10^{-2} M, ionic strength 0.1 M, T = 25 °C, Ar atmosphere.

The pH dependence of step II is summarized in Figures 10 and 11 for the reaction at 390 and 470 nm, respectively. The absorbance increase observed at 390 nm reaches a maximum value at pH = 2.2, and k_{obs} exhibits a sigmoid-shaped pH dependence to reach a limiting value of ca. 33 s^{-1} at pH > 2.5. In fact, the pH dependence of the absorbance increase is very similar to the [total S(IV)] dependence found at pH = 2.4 (see Figure 8a) and can be interpreted in a similar way. A variation in pH will affect

(25) Martinez, P.; Mohr, R.; van Eldik, R. *Ber. Bunsen-Ges. Phys. Chem.* **1986**, *90*, 609.

Scheme I

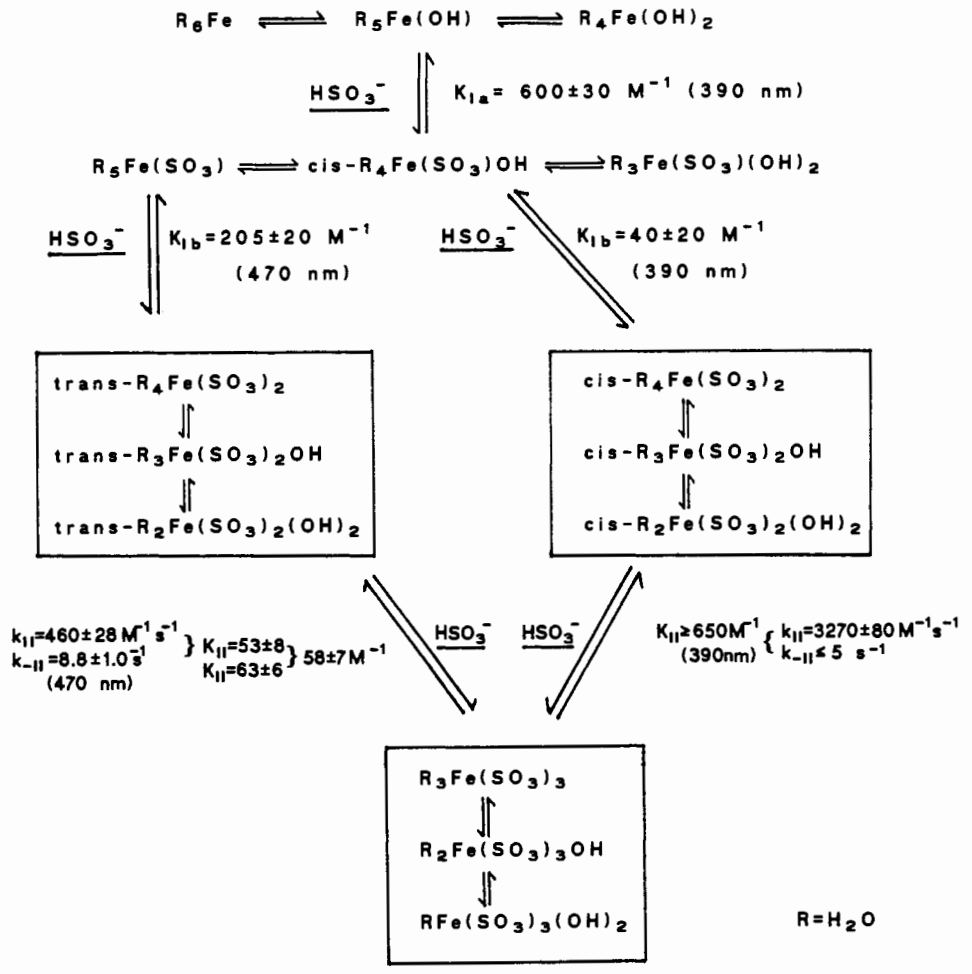

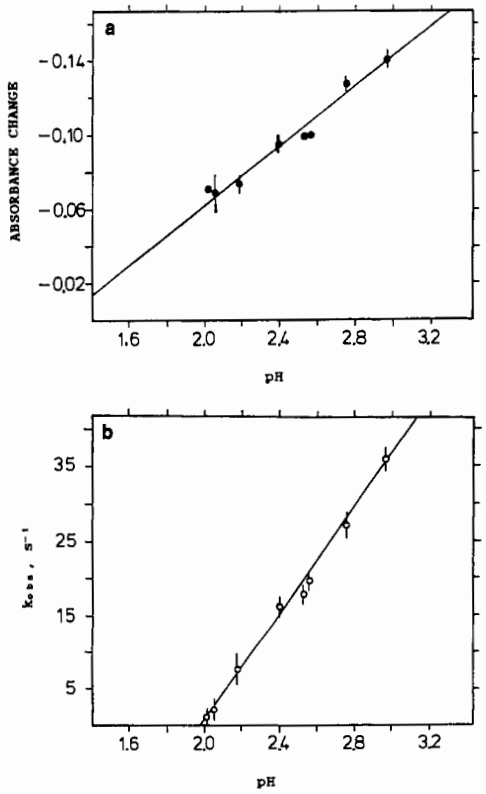

Figure 11. pH dependence of step II at 470 nm: (a) absorbance change as a function of pH; (b) k_{obs} as a function of pH. Conditions: [Fe(III)] = 5×10^{-4} M, [total S(IV)] = 2×10^{-2} M, ionic strength 0.1 M, T = 25 °C, Ar atmosphere.

the product distribution reached during step I and in that way determine the extent to which the reaction can proceed during step II. The sigmoid-shaped pH dependence of k_{obs} is characteristic for an acid–base equilibrium during which a more reactive hydroxo species of the 1:2 complex is produced. The tailing-off effect observed at lower pH (see Figure 10b) is probably due to the interference of equilibrium 4 in this pH range. The intercept at low pH can be due to a contribution either from a parallel process involving SO_2 uptake or from a reverse reaction. In contrast to these observations, the absorbance decrease observed during step II at 470 nm and the value of k_{obs} increase linearly with increasing pH (see Figure 11). No maxima are reached in either dependency, and the reaction only occurs at pH ≥ 2.0. The reaction at this wavelength is ca. 2 times slower than at 390 nm since double the [total S(IV)] was employed for the data in Figure 11b. The greater absorbance decrease with increasing pH is in good agreement with the lesser absorbance increase observed for pH ≥ 2 at 390 nm (Figure 10a) and therefore accounts for the other reaction path observed under such conditions. The linear increase in k_{obs} with increasing pH is once again ascribed to an acid–base equilibrium for which the pK_a value is significantly higher than 3.0, with some interference from equilibrium 4 as suggested above.

A study of step II in O_2-saturated solutions revealed spectral changes very similar to those reported in Figure 8a. Plots of k_{obs} versus [total S(IV)] under such conditions indicate a linear increase in k_{obs} with increasing concentration without the intercept observed in Figure 8b. The rate constants do not differ significantly, but the disappearance of the reverse step indicates that the product produced during step II does react with dissolved oxygen most probably to produce an oxo sulfito complex (see further discussion). The temperature dependence of step II was studied at 390 and 470 nm, and the results (Figure 12) suggest the following acti-

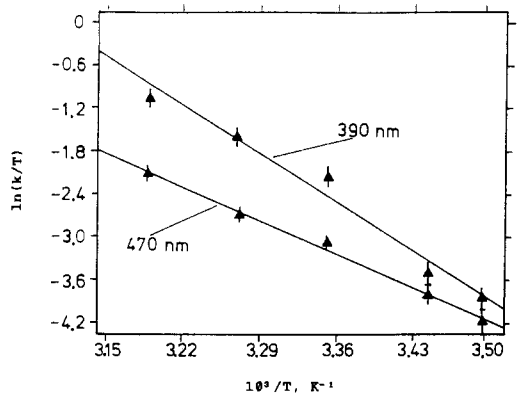

Figure 12. Temperature dependence of step II. Conditions are the same as for Figure 10.

vation parameters: 390 nm, $\Delta H^{\ddagger} = 80 \pm 8$ kJ mol^{-1}, $\Delta S^{\ddagger} = 49 \pm 25$ J K^{-1} mol^{-1}; 470 nm, $\Delta H^{\ddagger} = 56 \pm 3$ kJ mol^{-1}, $\Delta S^{\ddagger} = -38 \pm 9$ J K^{-1} mol^{-1}. It is important to note that these parameters were calculated from the temperature dependence of k_{obs} at a specific pH and [total S(IV)] and therefore represent overall effects. Nevertheless, the significant difference in especially $\Delta S^{\ddagger}$ is of mechanistic importance.

Suggested Mechanism. The overall simplified mechanism is presented in Scheme I. A number of simplifications are included: R represents a coordinated water molecule; no protons are included in the acid–base equilibria; no overall charges are included on the complexes due to uncertainties in the exact nature of the various complex species. This scheme can account for the spectroscopic and kinetic observations reported above. The uncertainties involved will be discussed in a detailed treatment of the individual steps.

Step I of the mechanism involves the rapid formation of 1:1 and 1:2 Fe(III)–S(IV) species during the reaction of $Fe(H_2O)_5OH^{2+}$ with HSO_3^-. The 1:1 species can be formulated as $Fe(H_2O)_5SO_3^+$, *cis*-$Fe(H_2O)_4(SO_3)(OH)$, or $Fe(H_2O)_3(SO_3)(OH)_2^-$. Although it is reasonable to assume that substitution will occur in the position trans to the hydroxy ligand, subsequent deprotonation is suggested to occur cis to the sulfite ligand due to the expected trans-labilization effect of the latter. The acid dissociation constant of the $Fe(H_2O)_5SO_3^+$ intermediate is unknown, but it is reasonable to assume that we are not dealing with a bisulfito complex. The pK_a values of coordinated ligands are in general some units lower than for the uncoordinated species,[7] which would suggest the pK_a of coorinated bisulfite to be lower than 2. The 1:1 complex can undergo a rapid subsequent substitution reaction to produce *cis*- or *trans*-$Fe(H_2O)_4(SO_3)_2^-$. The trans-labilization effect of coordinated sulfite has been observed in other studies.[12,13] It follows that it is realistic to suggest the formation of two 1:2 complexes; their concentration ratio will depend on the pH and [total S(IV)] employed. Once again the degree of deprotonation of the coordinated water molecules cannot be specified, neither can we comment in detail on the coordination geometry of these species. The FT-IR measurements suggest the formation of S-bonded sulfito complexes. Furthermore, the subsequent behavior of these complexes (step II) suggests that the interconversion of the cis and trans forms is slow and does not occur on the time base of the formation process. The spectroscopic measurements suggest that $K_{Ia} = 600 \pm 30$ M^{-1}, K_{Ib}(390 nm) $= 40 \pm 20$ M^{-1}, and K_{Ib}(470 nm) $= 205 \pm 20$ M^{-1}. Rate constants for this step lie between 500 and 10^3 s^{-1} and prevent a detailed kinetic analysis.

During step II the *cis*- and *trans*-bis(sulfito) species undergo subsequent substitution by HSO_3^- or SO_3^{2-} to produce a common tris(sulfito) species. The UV–vis spectrum of this species could be recorded in a rapid-scan experiment (Figure 13) and consists of a broad shoulder between 400 and 500 nm. The redox instability of this species (steps III and IV in Figure 1) does not allow a detailed study of the acid–base properties and the coordination geometry. On the basis of the trans-labilization ability of coordinated sulfite,[7] the *cis*-bis(sulfito) complex should be the more labile species and produce the 1:3 product with a higher yield,

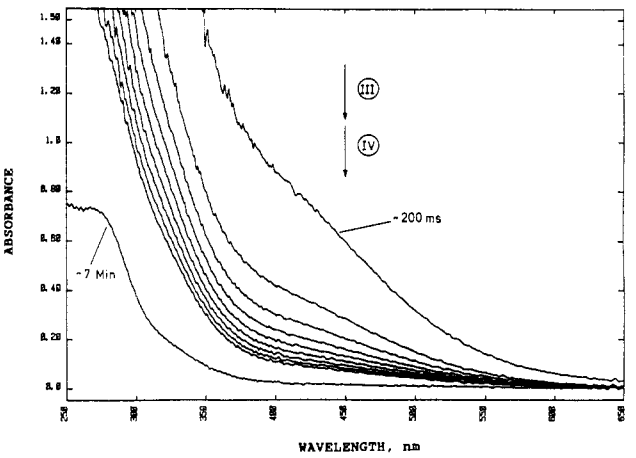

Figure 13. Spectral changes observed during steps III and IV. Conditions: [Fe(III)] = 2.5×10^{-3} M, [total S(IV)] = 5×10^{-3} M, pH = 2.0, ionic strength 0.1 M, $T = 25$ °C, $\Delta t = 10$ s.

i.e., K_{II}. On the basis of this argument the absorbance changes and kinetic data measured at 390 nm must be ascribed to the reaction of the *cis*-bis(sulfito) species and those measured at 470 nm to the *trans*-bis(sulfito) species. Thus, $K_{II} = 650$ M^{-1} at 390 nm and ca. 60 M^{-1} at 470 nm. The formation rate constants are 3.3×10^3 and 4.4×10^2 M^{-1} s^{-1} for the cis (390 nm) and trans (470 nm) reactions at pH 2.5, respectively. The similarity of the intercepts in Figures 8 and 9, i.e., rate constants for the reverse reaction of the tris(sulfito) species, underlines the fact that we are dealing with a single product species as suggested in Scheme I. No evidence for the formation of hydroxo- or sulfite-bridged complexes was found under the selected conditions. The pH dependence of step II can be interpreted in terms of the acid–base equilibria indicated in Scheme I. In this respect it is interesting to note that the substitution reactions of the *trans*-bis(sulfito) complex should exhibit a more distinct pH dependence since the formation of a hydroxo species will enhance substitution trans to this group, an effect not so important for the *cis*-bis(sulfito) complex. We assume that the trans species will exhibit a lower pK_a value characteristic for coordinated H_2O, whereas the cis species will exhibit a higher pK_a value due to the trans-labilizing effect of the sulfito ligands. The results in Figures 10 and 11 tend to support this expectation. The temperature dependence of step II reveals signifcantly different values for $\Delta S^{\ddagger}$ for the reactions of the *cis*- and *trans*-bis(sulfito) complexes. The positive value found for the cis complex (390 nm) supports a dissociatively activated substitution mechanism, whereas the negative value for the trans complex (470 nm) is more in line with an associative mechanism. This trend is furthermore in good agreement with the higher reactivity of the cis species, since the trans-labilization effect of the coordinated sulfite ligands will favor a more dissociative reaction mode.

The main reactions in Scheme I that are of kinetic significance can be summarized as

$$Fe(H_2O)_5OH^{2+} + HSO_3^- \rightleftharpoons Fe(H_2O)_5SO_3^+ + H_2O$$

$$Fe(H_2O)_5SO_3^+ \rightleftharpoons cis\text{-}Fe(H_2O)_4(SO_3)OH + H^+$$

$$Fe(H_2O)SO_3^+ + HSO_3^- \rightleftharpoons trans\text{-}Fe(H_2O)_4(SO_3)_2^- + H_3O^+$$

$$cis\text{-}Fe(H_2O)_4(SO_3)OH + HSO_3^- \rightleftharpoons cis\text{-}Fe(H_2O)_4(SO_3)_2^- + H_2O$$

$$trans\text{-}Fe(H_2O)_4(SO_3)_2^- + HSO_3^- \rightleftharpoons Fe(H_2O)_3(SO_3)_3^{3-} + H_3O^+$$

$$cis\text{-}Fe(H_2O)_4(SO_3)_2^- + HSO_3^- \rightleftharpoons Fe(H_2O)_3(SO_3)_3^{3-} + H_3O^+$$

This scheme accounts for steps I and II of the overall process and is based on the fact that $Fe(H_2O)_5OH^{2+}$ and HSO_3^- are the main reactive species that initiate the initial and subsequent substitution reactions. The acid–base equilibria and stereochemistry of the subsequent reactions are controlled by the trans-labilizing effects

of coordinated sulfite and hydroxide ions. In both cases trans labilization of coordinated water will lead to a weakening of the metal–water bond and strengthening of the O–H bond, i.e., an increase in pK_a. Although *cis*-$Fe(H_2O)_4(SO_3)OH$ can produce both *cis*- and *trans*-bis(sulfito) complexes on subsequent substitution, the latter species can only interconvert on a much slower time scale. The overall formation constant of the 1:3 complex can be expressed as $K_{Ia}[K_{Ib}(470\ nm)][K_{II}(470\ nm)] = 7 \times 10^6\ M^{-3}$ (via trans species) or $K_{Ia}[K_{Ib}(390)\ nm)][K_{II}(390\ mm)] = 16 \times 10^6\ M^{-3}$ (via cis species).

The $Fe(H_2O)_4(OH)_2^+$ complex is not considered as a reactive species in Scheme I, since at higher pH less labile hydroxo-bridged complexes are produced. These will interact with the S(IV) species, but on a slower time scale than steps I and II. They are therefore considered to play a significant role in the slower subsequent decomposition reactions and especially account for step IV (see part 2).[6]

Comparison with Available Data. In a recent detailed study on the kinetics of Fe(III)–S(IV) transients,[26] performed while this work was in progress, the authors report stopped-flow spectroscopic evidence for two subsequent formation reactions of Fe(III)–S(IV) transients. They report half-lives of less than 3 and 30 ms for the two steps, respectively, which is in good agreement with our findings (Figure 1). Other qualitative observations also agree with the results reported here. The authors interpret their data in terms of the formation of a 1:1 complex, the fast reaction being due to substitution of $Fe(H_2O)_5OH^{2+}$ and the slow reaction being due to a subsequent linkage isomerization step. Their overall formation constant of 67 ± 10 M^{-1}, measured at 350 and 450 nm, is in good agreement with our values of 40 ± 20 M^{-1} for $K_{Ib}(390\ nm)$ and ca. 60 M^{-1} for $K_{II}(470\ nm)$.

Other studies in the literature support our finding of Fe(III)–S(IV) species of varying coordination number. Danilczuk and Swinarski[27] investigated the spectroscopic behavior of Fe(III)–S(IV) mixtures immediately after mixing and conclude that there is formation of 1:1, 1:2, and 1:3 complexes at pH = 2–3. Other authors have also reported the formation of 1:1 and 1:2 complexes and do not exclude the possible formation of a 1:3 species.[28-32] The inability of other groups to detect higher substituted species than 1:1 complexes can often be understood when the selected experimental conditions are compared to those adopted in the present study.[33,34] Many investigators do not consider the complex formation at all and interpret their data in terms of a reaction sequence initiated by electron transfer between Fe(III) and HSO_3^-/SO_3^{2-}.

The next important aspect to consider is the selection of the reactive Fe(III) species. We have outlined above that $Fe(H_2O)_5OH^{2+}$ is orders of magnitude more labile than $Fe(H_2O)_6^{3+}$[24,25] and therefore prefer this species as the main reaction center in Scheme I. Many investigators have studied the substitution reactions of $Fe^{III}(aq)$ with a variety of entering ligands and ascribe the strong $[H^+]$ dependence of such reactions to the participation of the monohydroxo species. The substitution mechanisms of the $Fe(H_2O)_6^{3+}$ and $Fe(H_2O)_5OH^{2+}$ species differ considerably as demonstrated by the volumes of activation for these reactions.[24,25,35] The more reactive hydroxo complex exhibits positive volumes of activation and undergoes substitution according to a dissociative mechanism, whereas the substitution reactions of the hexaaqua complex exhibit negative volumes of activation and proceed according to an associative mechanism.[24,25,35] The trans-labilization effect of the hydroxo ligand presumably enhances the substitution rate of the $Fe(H_2O)_5OH^{2+}$ species. A similar trend was observed for the substitution behavior of the bis(sulfito) transients, where the higher reactivity of the cis complex can also be associated with a trans-labilization effect of coordinated sulfite and a corresponding dissociative substitution mode. The rates of formation of the 1:1 and higher substituted sulfito complexes, as calculated from the [total S(IV)] dependence of k_{obs}, are in good agreement with those reported in the literature for substitution by Cl^-, Br^-, SCN^-, and similar nucleophiles,[36] especially when the difference in nucleophilicity is taken into account. The value of k_1 (slope of Figure 6) is such that it favors substitution of $Fe(H_2O)_5OH^{2+}$ by HSO_3^-. Finally, the value of k_{II} (ca. $3.3 \times 10^3\ M^{-1}\ s^{-1}$ at pH 2.5 and 390 nm) for the substitution of the *cis*-bis(sulfito) complex by sulfite is a realistic number for a reaction induced by a trans-labilization effect of coordinated sulfite. The corresponding value of $4.6 \times 10^2\ M^{-1}\ s^{-1}$ for the *trans*-bis(sulfito) complex also fits into the overall picture of substitution behavior of Fe(III) complexes. These observations are all in line with the S-bonded nature of the sulfito complexes, although no definite proof is presently available, especially in light of the fact that $(NH_4)_9[Fe(SO_3)_6]$ only contains O-bonded sulfite ligands.[37]

The results of this study are in good agreement with those found for labile Pd(II) complexes,[14,15] where substitution of an aqua ligand resulted in the formation of an S-bonded sulfito complex. This species exhibited strong labilization effects and resulted in the loss of the coordinated ammine ligand followed by sulfite substitution to produce a bis(sulfito) complex. These trends completely contrast with those found for nonlabile metal centers, where metal hydroxo species undergo SO_2 uptake to produce O-bonded sulfito species without metal–oxygen bond breakage.[7] We therefore conclude that SO_2 uptake by $Fe(H_2O)_5OH^{2+}$ to produce $Fe(H_2O)_5OSO_2^+$, presumably followed by a slow intramolecular linkage isomerization to the S-bonded species, is considerably slower than direct substitution of a very labile coordinated water molecule to produce the S-bonded species.

A complete account of the decomposition reactions of the Fe(III)–sulfito complexes is presented in part 2 of this series.[6]

Acknowledgment. We gratefully acknowledge financial support from the Deutsche Forschungsgemeinschaft, the Fonds der Chemischen Industrie, and the Scientific Affairs Division of NATO under Grant No. RG. 0681/85. Drs. M. R. Hoffman and M. H. Conklin are thanked for providng preprints of their papers prior to publication. We acknowledge the assistance of Dr. Achim Gerhard (Max Planck Institute for Biophysics, Frankfurt, FRG) with some of the kinetic measurements.

Registry No. $Fe(H_2O)_5OH^{2+}$, 15696-19-2; HSO_3^-, 15181-46-1.

(26) Conklin, M. H.; Hoffmann, M. R. *Environ. Sci. Technol.* **1988**, *22*, 899.
(27) Danilczuk, E.; Swinarski, A. *Rocz. Chem.* **1961**, *35*, 1563.
(28) Bassett, H.; Parker, W. G. *J. Chem. Soc.* **1951**, 1540.
(29) Freiberg, J. *Atmos. Environ.* **1975**, *9*, 661.
(30) Huie, R. E.; Peterson, N. C. In *Trace Atmospheric Constituents—Properties, Transformations and Fates*; Schwartz, S. E., Ed.; Wiley: New York, 1983.
(31) Hoffmann, M. R.; Boyce, S. D. In *Trace Atmospheric Constituents—Properties, Transformations and Fates*; Schwartz, S. E., Ed.; Wiley: New York, 1983.
(32) Hoffmann, M. R.; Jacob, D. J. In *SO_2, NO and NO_2 Oxidation Mechanisms; Atmospheric Considerations*; Calvert, J. G., Ed.; Butterworths: London, 1984.
(33) Carlyle, D. W. *Inorg. Chem.* **1971**, *10*, 761.
(34) Kanaker, D. G. *J. Phys. Chem.* **1963**, *67*, 871.
(35) Funahashi, S.; Ishihara, K.; Tanaka, M. *Inorg. Chem.* **1983**, *22*, 2070.
(36) Grant, M.; Jordan, R. G. *Inorg. Chem.* **1981**, *20*, 55.
(37) Larsson, L. O.; Niinisto, L. *Acta Chem. Scand.* **1973**, *27*, 859.